Supporting Information

Doping Ru on FeNi LDH/$Fe^{II/III}$-MOF heterogeneous core-shell structure for efficient oxygen evolution

Yijia Cao[1], Yusong Wen[1],Yanrong Li[1], Mengya Cao[1], Bao Li[1], Qing Shen[1] and Wen Gu[1,*]

[1]College of Chemistry, Key Laboratory of Advanced Energy Materials Chemistry (MOE), Tianjin Key Laboratory of Metal and Molecule Based Material Chemistry, Collaborative Innovation Centre of Chemical Science and Engineering, Nankai University, Tianjin 300071, China

* Corresponding author.

E-mail address:
guwen68@nankai.edu.cn

Characterizations.

In this paper, XRD tests were completed by polycrystalline X-ray diffractometer (Rigaku, Japan, SmartLab 9Kw) with a Cu Kαirradiation source (λ = 1.5406 Å). The tube voltage was 40 kV, the tube current was 150 mA, and the expected resolution was 0.02 degree/step. The range of scanning angle was 5-80°, and the scanning speed was 5°/min. The X-ray powder diffraction card could be used to find the crystal plane index (hkl) and crystal plane spacing (d) of each diffraction crystal plane. The analytical test software jade 6.5 was used to determine the composition of the materials. Scanning Electron Microscope (ZEISS, MERLIN Compact, Germany) has a resolution of 1.6 nm at 1 kV acceleration voltage and can reach 0.8 nm at 30 kV acceleration voltage in STEM mode. And it can be used with energy dispersive spectrum (EDS). The acceleration voltage is 5 kV in morphology test and 20 kV in EDS test. High Resolution Transmission Electron Microscope (FEI, Talos F200X G2) is used to observe the internal structure of materials and determine the crystallization of materials. The crystal condition, crystal shape and crystal surface of the material can be obtained by analyzing the lattice fringe of the material. The information resolution of the instrument is 0.12 nm at acceleration voltage of 200 kV. X-ray Photoelectron Spectroscopy (XPS, Thermo Scientific K-Alpha) uses Al Kα ray as an excitation source, with a photoelectron energy of 1486.6 eV. The

working voltage is 12 kV and the filament current is 6 mA. The full spectrum test energy is 150 eV and the step size is 1 eV. Narrow-spectrum scanning has a pass energy of 50 eV and a step size of 0.1 eV. Surface contamination C 1s (284.8 eV) was used as the modification standard for binding energy. Raman spectra were recorded by a Thermo Fischer DXR Raman spectrometer with a laser wavelength of 532 nm of an Ar-ion laser from 50 cm^{-1} to 4000 cm^{-1}.

Electrochemical Measurements.

2.5 mg of catalytic materials and 2.5mg of catalytic materials were added to the mixed solution composed by 660 μL of water, 330 μL of ethanol and 10 μL of Nafion to form the inks. After full ultrasonic dispersion for two hours, 5 μL of the inks were uniformly droped on glassy carbon electrodes with a diameter of 3 mm and dried with an infrared light source. In a typical three-electrode system, a Hg/HgO of double salt bridge is used as a reference electrode, a carbon rod is used as counter electrode and the glassy carbon electrode loaded with catalytic materials as the working electrode. All electrochemical measurements were performed in 1.0 M KOH solution (pH=13.7) with a CHI660 electrochemical work station. Before all tests, 20-50 cycles of cyclic voltammetry (CV) was scanned until a stable Linear sweep voltammetry (LSV) curve was obtained. The scanning rate of LSV is 5 mV/s, and the iR-compensation is 95%. All the electrode potentials with

reference to the reference electrode are converted to reversible hydrogen electrode potential (RHE) by Nernst equation：

$$E(RHE) = E(Hg/HgO) + 0.059*13.7\ V + 0.098\ V$$

Tafel slops were fitted by LSV curve of electrode materials before and after 10 mA/cm^2. Electrochemical impedance spectroscopy (EIS) tests were performed at 0.60 V with a frequency ranging from 1 to 100,000 Hz, and the amplitude is 5 mV. The final impedance datas were obtained by fitting in the software ZVIEW. Double-layer capacitance (C_{dl}) was measured via different scanning rates (10 mV - 60 mV) of cyclic voltammograms (CV) in a potential range of 0.2 to 0.3 V to evaluate the electrochemically active surface areas (ECSA) of the electrocatalysts. The difference between the highest and lowest current density of CV curves at 0.25V under different scanning speeds is calculated, and then linearly fitted with the scanning speeds, and the obtained slope is C_{dl}. The relationship between C_{dl} and ECSA is as the formula:

$$ECSA = C_{dl}/C_s\ (Cs = 40\ mF/cm^2)$$

The continuous amperometric i-t testing was conducted at about 10 mA/cm^2 at 0.60 V without iR-compensation.

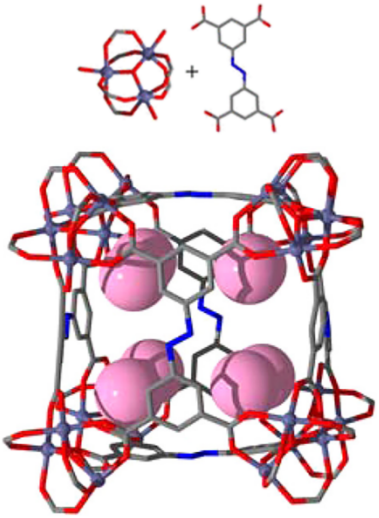

Figure S1. The structural schematic diagram of Fe-soc-MOF. (Color code: C = light gray, O = red, N = blue, Cl = pink, and Fe = dark green.) [S1]

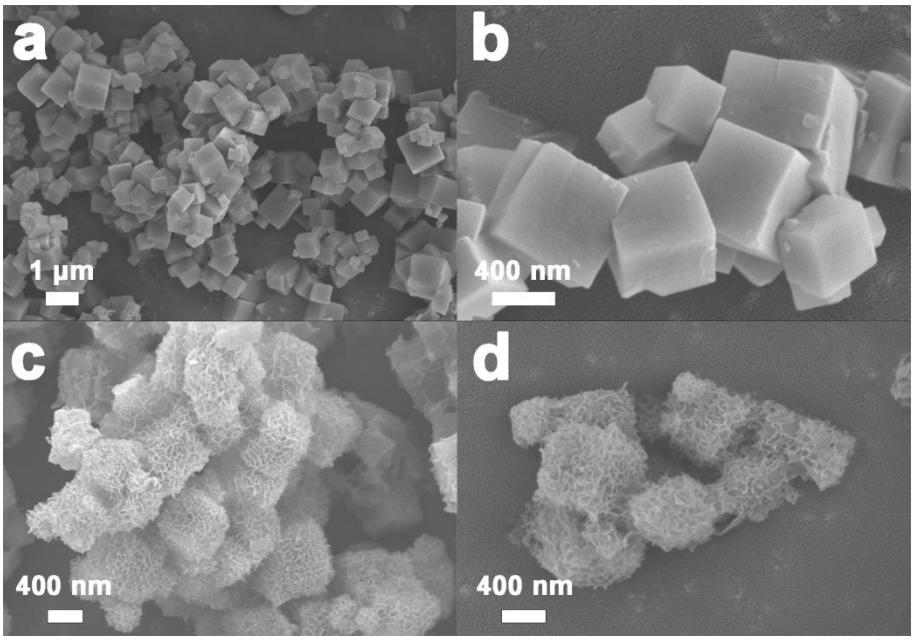

Figure S2. SEM images of (a-b) Fe-soc-MOF and (c-d) FeNi LDH/MOF.

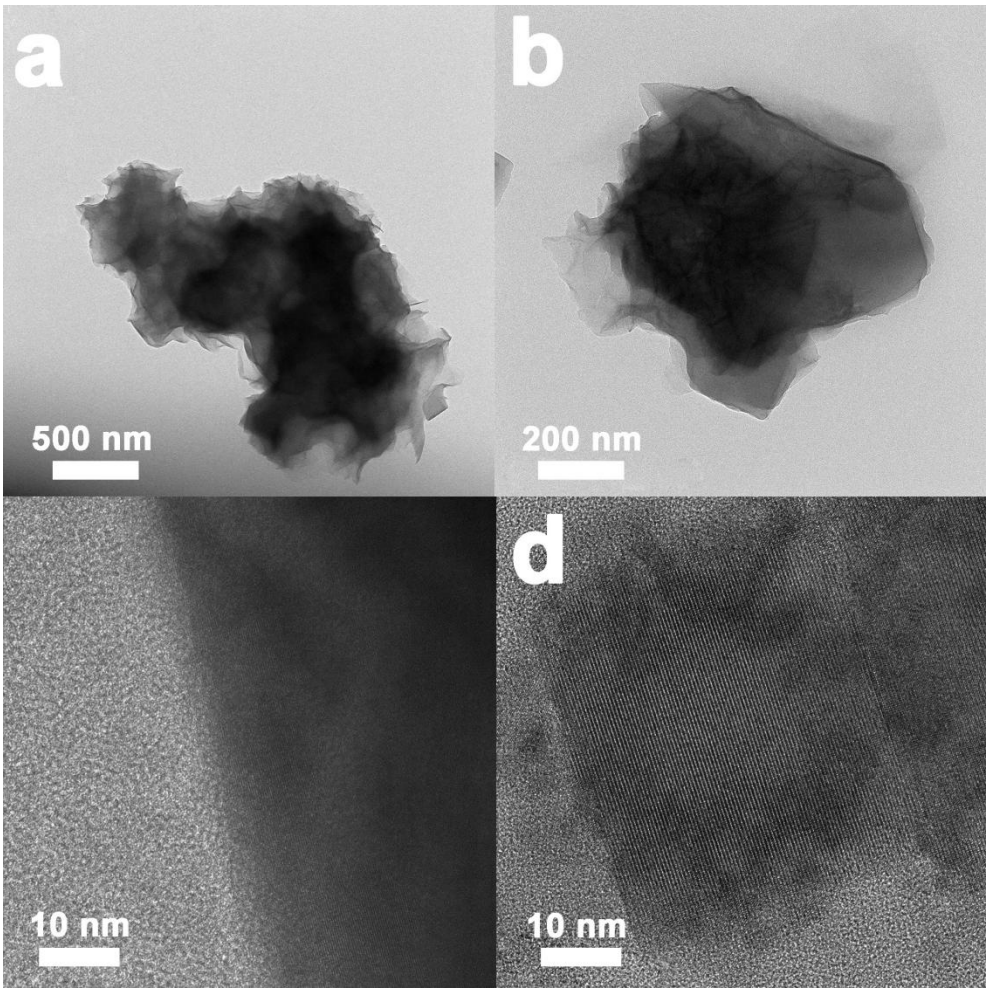

Figure S3. (a-b) scanning TEM images and (c-d) High-resolution of FeNi LDH/MOF.

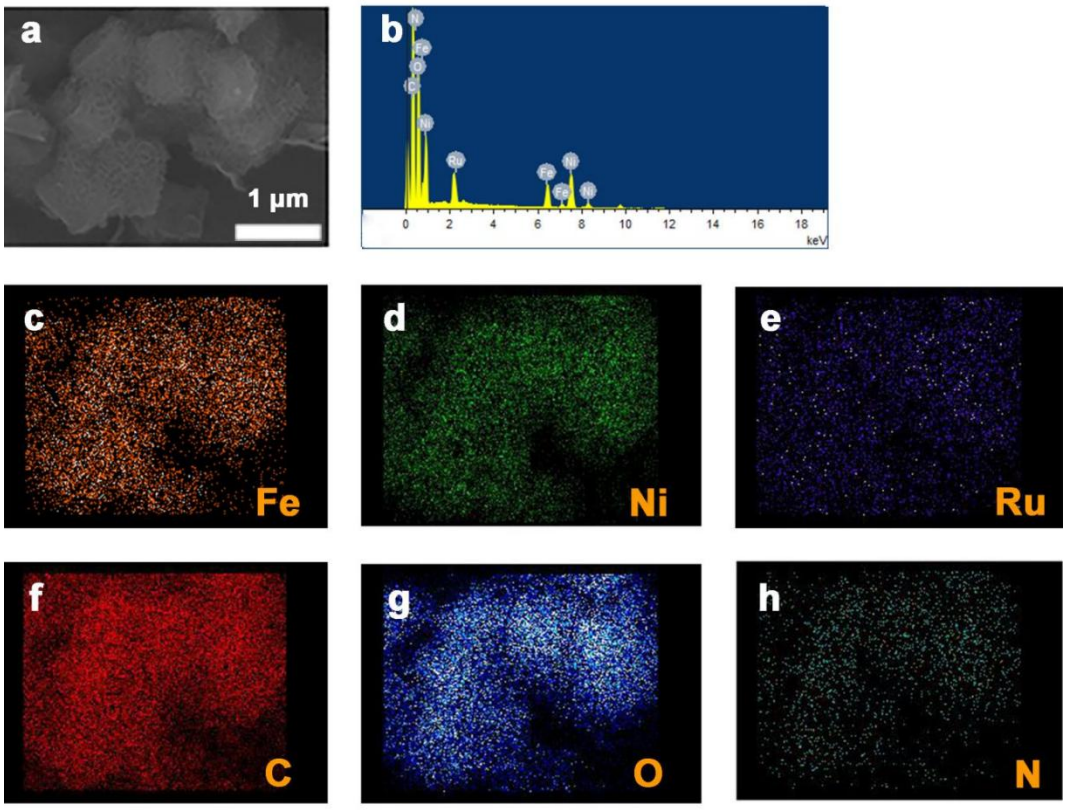

Figure S4. (a) SEM image (b) EDX pattern and (c-h) corresopnding elemental mapping images of Ru@FeNi LDH/MOF.

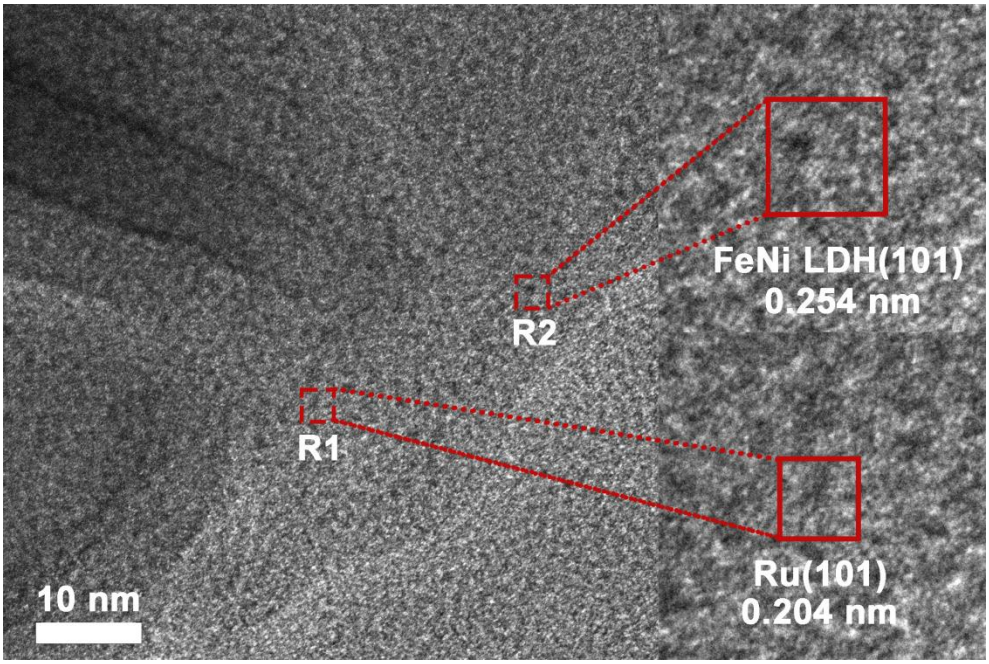

Figure S5. HRTEM image of Ru@FeNi LDH/MOF.

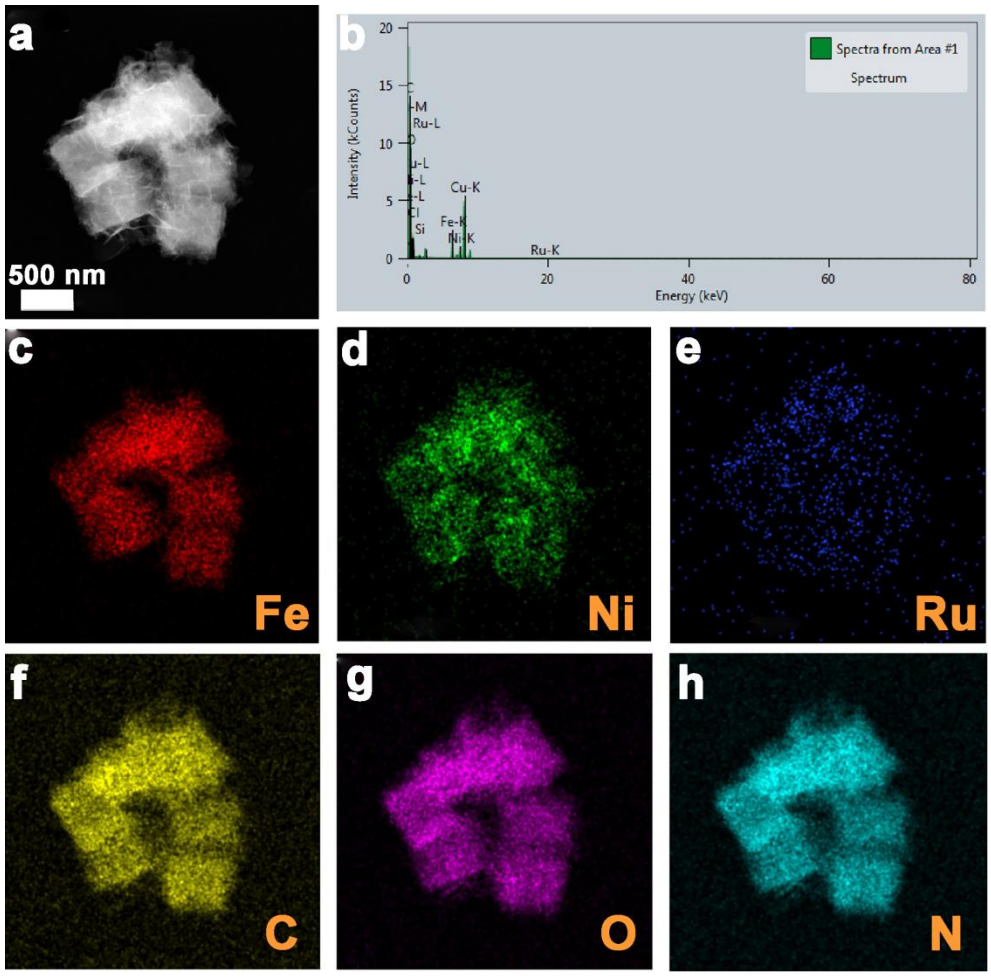

Figure S6. (a) TEM image (b) EDX pattern and (c-h) corresopnding elemental mapping images of Ru@FeNi LDH/MOF.

Sample	Fe (wt%)	Ni (wt%)	Ru (wt%)
Ru@FeNi LDH/MOF	11.64	17.43	4.23

Table S1. The content of Fe, Ni and Ru of Ru@FeNi LDH/MOF by ICP

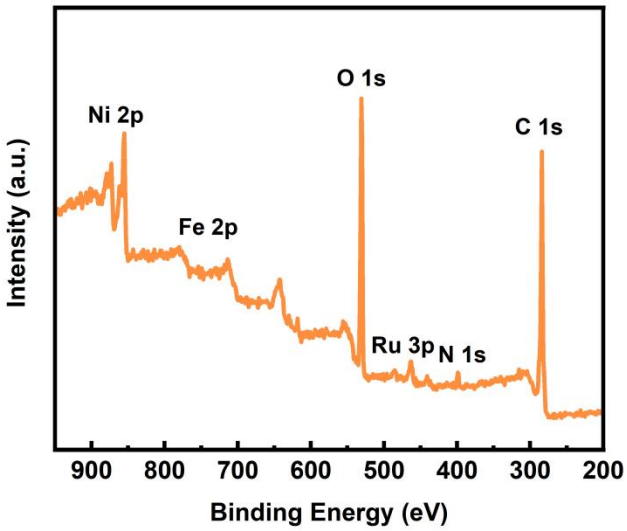

Figure S7. Full spectrum X-ray photoelectron spectroscopy (XPS) spectra of Ru@FeNi LDH/MOF.

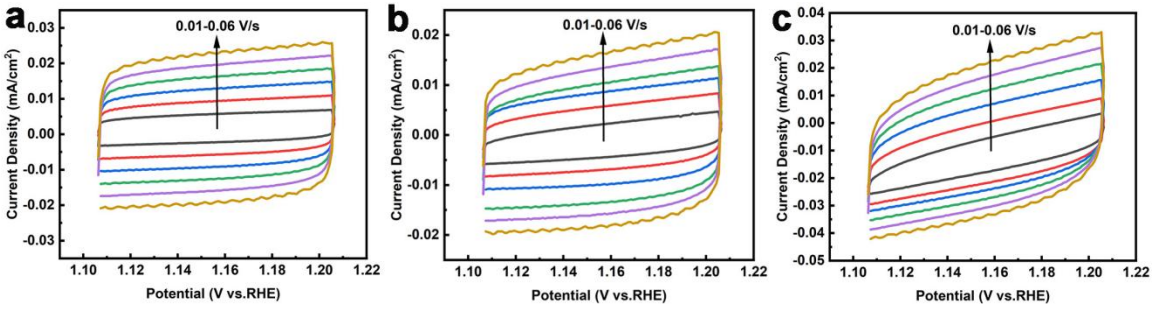

Figure S8. The CV curves of (a) Fe-soc-MOF, (b) FeNi LDH/MOF and (c) Ru@FeNi LDH/MOF at different scan rate of 10, 20, 30, 40, 50 and 60 mV/s.

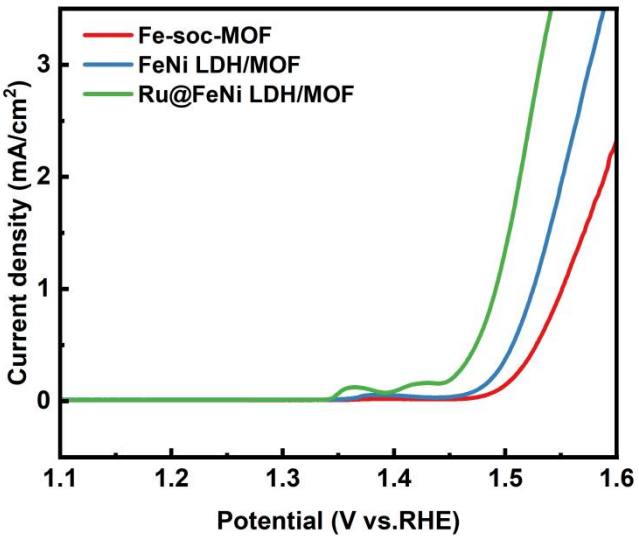

Figure S9. ECSA-normalized LSV curves for Ru@FeNi LDH/MOF, FeNi LDH/MOF and Fe-soc-MOF during OER process.

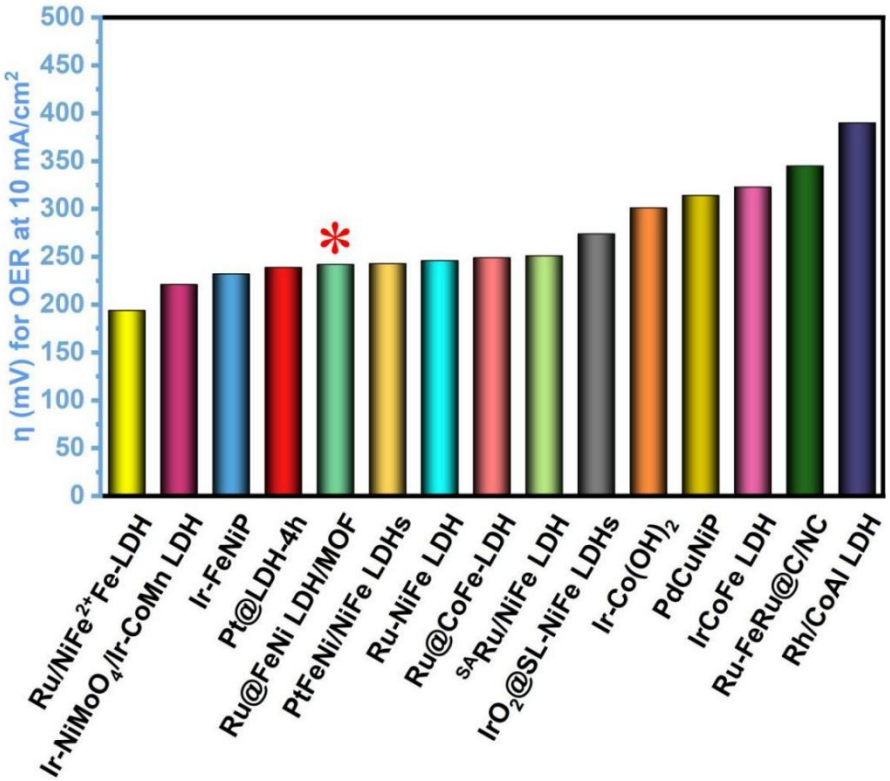

Figure S10. Comparison of the overpotential at 10 mA/cm^2 for Ru@FeNi LDH/MOF with recently reported non-self-supporting noble-metal-attached transition metal based OER electrocatalysts.

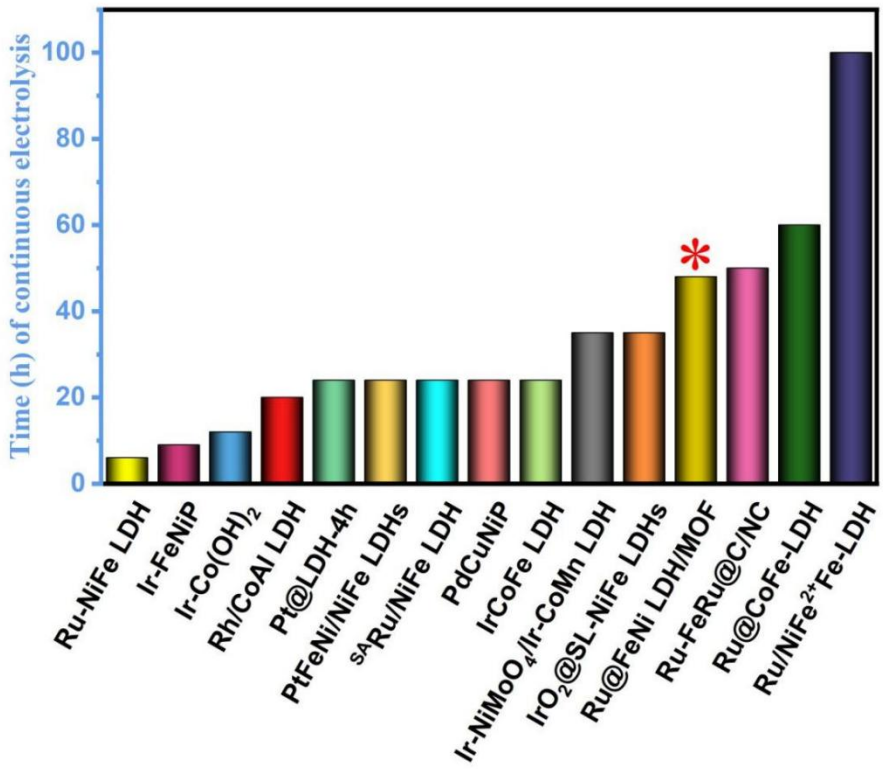

Figure S11. Comparison of the time of continuous electrolysis for Ru@FeNi LDH/MOF with recently reported non-self-supporting noble-metal-attached transition metal based OER electrocatalysts.

Electrocatlyst	Electrolyte	Overpotential (mV) η_{10}	Stability （h）	References
Ru@FeNi LDH/MOF	1.0 M KOH	242	48	This Work
Ru/NiFe^{2+}Fe-LDH	1.0 M KOH	194	100	S2

Ir-$NiMoO_4$/Ir-CoMn LDH	1.0 M KOH	221	35	S3
Ir-FeNiP	1.0 M KOH	232	9	S4
Pt@LDH-4h	1.0 M KOH	239	24	S5
PtFeNi/NiFe LDHs	1.0 M KOH	243	24	S6
Ru-NiFe LDH	1.0 M KOH	246	6	S7
Ru@CoFe-LDH	1.0 M KOH	249	60	S8
^{SA}Ru/NiFe LDH	1.0 M KOH	251	24	S9
IrO_2@SL-NiFe LDHs	1.0 M KOH	274	35	S10
Ir-$Co(OH)_2$	1.0 M KOH	301	12	S11
PdCuNiP	1.0 M KOH	314	24	S12
IrCoFe LDH	1.0 M KOH	323	24	S13
Ru-FeRu@C/NC	1.0 M KOH	345	50	S14
Rh/CoAl LDH	1.0 M KOH	390	20	S15

Table S2. Comparison of activation energies of FeNiP and FeNiP/NC at each reaction step in OER pathway.

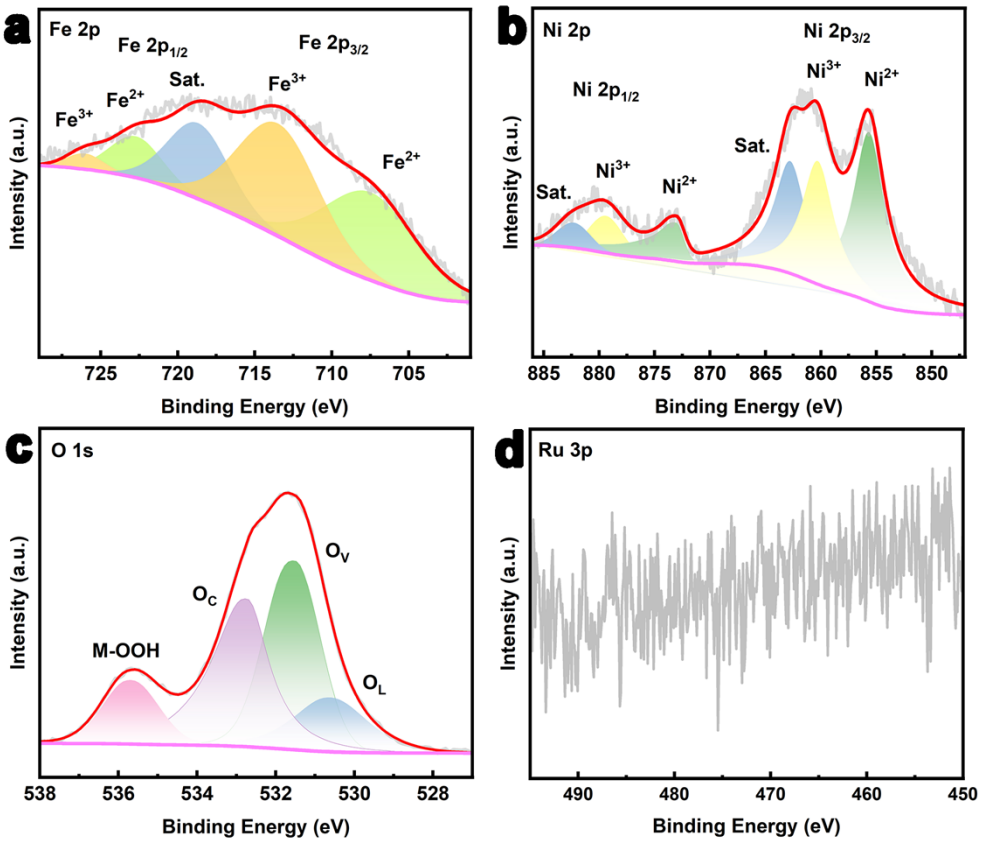

Figure S12. High-resolution XPS of (a) Fe 2p, (b) Ni 2p, (c) O 1s and (d) Ru 3p for Ru@FeNi LDH/MOF after high current stability test.

References

(S1) A. J. Cairns, J. Eckert, L. Wojtas, et al, Chemistry of Materials, 2016, **28**, 7353-7361.

(S2) X. Duan, P. Li, D. Zhou, et al, Chemical Engineering Journal, 2022, **446**, 136962.

(S3) S. Tang, Y. Zhou, X. Lu, et al, Journal of Alloys and Compounds, 2022, **924**, 166415.

(S4) N. Yang, S. Tian, Y. Feng, et al, Small, 2023, **19**, 2207253.

(S5) J. Huo, Z. Ma, Y. Wang, et al, Small, 2023, **19**, 2207044.

(S6) G. Huang, Y. Li, R. Chen, et al, Chinese Journal of Catalysis, 2022, **43**, 1101-1110.

(S7) Y. Yang, W. Wang, Y. Yang, et al, Journal of The Electrochemical S.ciety, 2022, **169**, 024503.

(S8) A. Karmakar, R. Jayan, A. Das, et al, ACS Applied Materials & Interfaces, 2023, **15**, 26928-26938.

(S9) Y. Yang, Q. Yang, Y. Yang, et al, ACS Catalysis, 2023, **13**, 2771-2779.

(S10) D. Lia, T. Li, G. Hao, et al, Chemical Engineering Journal, 2020, **399**, 125738.

(S11) Z. Li, D. Liu, X. Lu, et al, Dalton Transactions, 2022, **51**, 1527-1532.

(S12) Y. Zheng, R. Guo, X. Li, et al, Frontiers in Chemistry, 2023, **11**, 1122333.

(S13) J. M. Yu, J. Song, Y. K. Kim, et al, Nano Letters, 2023, **23**, 5092-5100.

(S14) W. Feng, Y. Feng, J. Chen, et al, Chemical Engineering Journal, 2022, **437**, 135456.

(S15) Y. Li, X. Wang, X. Han, et al, ACS Applied Nano Materials, 2023, **6**, 7984-7991.